Model for the Thermodynamic Properties of a Biodiesel Fuel

Marcia L. Huber, Eric W. Lemmon, Andrei Kazakov, Lisa S. Ott,† and Thomas J. Bruno*

Thermophysical Properties Division National Institute of Standards and Technology Boulder, CO

Received February 23, 2009. Revised Manuscript Received May 16, 2009

We present an equation-of-state approach to modeling the thermodynamic properties of a biodiesel fuel. Preliminary Helmholtz-type equations of state were developed with limited experimental data for five fatty acid methyl esters (FAMEs) that are the primary constituents of soy-based biodiesel fuel, namely, methyl palmitate, methyl stearate, methyl oleate, methyl linoleate, and methyl linolenate. These components were combined in a mixture model using ideal mixing to represent the thermodynamic properties of a biodiesel fuel. We performed limited experimental measurements on the density, sound speed, and initial boiling point of two biodiesel fuel samples and compared the results with the model.

Introduction

Biodiesel fuel is a renewable fuel comprised of monoalkyl esters of long chain fatty acids. It can be produced from a variety of feedstocks including common vegetable oils (soybean, cottonseed, palm, peanut, canola, sunflower, safflower, coconut), animal fats (tallow), and even waste cooking oil.[1] In the United States, the predominant feedstock is soybeans.[2] The most common compounds present in soy-based biodiesels are the fatty acid methyl esters (FAMEs): methyl palmitate, methyl stearate, methyl oleate, methyl linoleate, and methyl linolenate.[3] It has recently been suggested that, by optimizing the relative abundance of FAMEs, one could conceivably develop "designer" biodiesel.[3] Furthermore, knowing the physical properties of a fuel can aid both in characterizing the fuel[4] as well as in optimizing engine efficiency.[5]

Biodiesel fuel consisting of primarily FAME constituents is referred to as B100.[6] This fluid is now typically used only as a blending stock, since most engine manufacturers will not certify engines to operate on B100. Also present in the market are various mixtures of B99, in which there is a small amount of petroleum-based diesel fuel. This is often present merely as a tank contaminant, or it can be found in an intentionally prepared mixture. B99 does not necessarily refer to a measured percentage, but merely a high level of FAME with traces of petroleum diesel fuel. More common mixtures that are sold for light and medium trucking, and the diesel automobile market, are B5 and B20. There are engines that can operate on these fuels without violation of warranty.

For biodiesel fuel to replace or extend petroleum-derived diesel fuel on a large scale, it is necessary to be able to substitute the two fuels in a fairly straightforward manner (that is, biodiesel fuel, or mixtures thereof, should ideally be drop-in replacements). As the market accepts the various blends of biodiesel fuel mentioned above, the availability of thermophysical property information will become more critical. It is impractical to measure such properties for all potential biodiesel fuel streams; thus, the development of thermodynamic models is needed to provide such a knowledge base. The goal of this work is to present a preliminary thermodynamic model for biodiesel fuels.

We note that, for the comparisons of our model with the real fuel, we used two separate samples of B100. At present, there are a very limited number of suppliers of B100 blending stocks. In our previous work on compositional and enthalpic variability,[7] we used four separate fluids for the comparison: three commercial stocks and one that we prepared ourselves from olive oil. One of the commercial stocks was found to be slightly contaminated with petroleum diesel, as we reported. Thus, this stock was not strictly B100, but rather B99. The real fuel comparisons presented in this paper are with the two commercial B100 stocks that contain only FAME constituents.

We proceed by first presenting the experimental measurements on biodiesel fuel samples, then developing equations of state for the pure fluid constituents of the fuel (incorporating previous experimental measurements[8]), formulating a mixture model, and finally comparing the model with the experimental results.

Experimental Section

Two B100 biodiesel samples were obtained from commercial sources. Both had soybean oil feedstocks and were compliant with ASTM D-6751.[6] The chemical compositions of the samples were determined[7] by the GC-MS method, and the results are given in Table 1. The estimated uncertainty (2σ) for the mole fractions is 0.001−0.002 mol fraction. The values reported in Table 1 do not sum exactly to unity, due to the presence of heavier FAMEs (methyl myristate, methyl arachidate, methyl behenate, and some heavier FAMEs) that were found in small or trace amounts.

* Corresponding author: e-mail: bruno@boulder.nist.gov; phone: 303-497-5158; fax: 303-497-5927.
† Present address: Department of Chemistry and Biochemistry, California State University, Chico CA.

(1) Knothe, G.; Van Gerpen, J.; Krahl, J. *The Biodiesel Handbook*; AOCS Press: Champaign, IL, 2005.
(2) Saraf, S.; Thomas, B. *Proc. Saf. Envir. Prot.* **2007**, *85*, 360–364.
(3) Knothe, G. *Energy Fuels* **2008**, *22*, 1358–1364.
(4) Castro, M. P. P.; Andrade, A. A.; Franco, R. W. A.; Miranda, P. C. M. L.; Sthel, M.; H., V.; Constantino, R.; Baesso, M. L. *Chem. Phys. Lett.* **2005**, *411*, 18–22.
(5) Moron-Villarreyes, J. A.; Soldi, C.; Amorim, A. M.; Pizzolatti, M. G.; Mendonca, A. P.; D'Oca, M. G. M. *Fuel* **2007**, *86*, 1977–1982.
(6) Standard specification for biodiesel fuel blend stock (B100) for middle distillate fuels, ASTM Standard D-6751−08. In Book of Standards; ASTM: 2008; Vol. 05−04.
(7) Ott, L. S.; Bruno, T. J. *Energy Fuels* **2008**, *22*, 2861–2868.
(8) Ott, L. S.; Huber, M. L.; Bruno, T. J. *J. Chem. Eng. Data* **2008**, *53*, 2412–2416.

10.1021/ef900159g
Published on Web 06/12/2009

Table 1. Chemical Composition of Two B100 Biodiesel Fuel Samples, in mol Fraction

	commercial sample A	commercial sample B
methyl palmitate	0.139	0.147
methyl stearate	0.087	0.121
methyl oleate	0.302	0.353
methyl linoleate	0.380	0.310
methyl linolenate	0.090	0.066

The densities and speeds of sound of the two fuels were measured concurrently with a commercial instrument equipped with a vibrating U-tube densimeter and pulse-echo velocity of sound measurement cell. Before each measurement, the instrument was calibrated with deionized degassed water at 20 °C; the reproducibility of the sound speed of water was within 0.01% before and after measurements of the biodiesels. After each calibration, the instrument was rinsed at least five times with each of two solvents (acetone and n-hexane), then maintained at 70 °C for 1 h under a stream of forced room air to ensure that the measurement cells were thoroughly cleaned and dried. The measurements were carried out at atmospheric pressure and over a temperature range of 278−333 K.

In earlier work[8] we measured the density and sound speed of the individual FAME constituents: methyl palmitate, methyl stearate, methyl oleate, methyl linoleate, and methyl linolenate. In the present work, we measured the boiling temperatures of these fluids with the same technique that is used to measure the initial boiling behavior of complex fluids while performing an advanced distillation curve measurement. The apparatus used for this, which has been presented in detail elsewhere,[9−13] consists of a distillation flask and head with thermocouples placed in the head and in the fluid. A stirrer is also placed in the fluid. Heating is provided with an aluminum enclosure that is fully insulated to provide uniform temperature control. Temperature control is provided with a programmable, model predictive controller that mimics the shape of a distillation curve. Direct observation through the distillation flask window or through an illuminated borescope facilitates these observations. During the early stages of a measurement the first bubbles will appear intermittently, and this action will quell if the stirrer is stopped momentarily. Sustained vapor bubbling is then observed, which is somewhat intermittent, but it is observable even when the stirrer is momentarily stopped. Finally, the temperature at which vapor is first observed to rise into the distillation head is observed. This is termed the vapor rise temperature. We have demonstrated that this is the actual boiling temperature of a fluid, and the initial boiling temperature of a mixture.

Experimental Results

The density and speed of sound measurements on the B100 fuel samples are reported in Tables 2 and 3. Each measurement of density and speed of sound was repeated four times for each of the biodiesel fuel samples. The expanded total uncertainty (with a coverage factor of $k = 2$, incorporating both random and systematic uncertainty) in each measurement is given parenthetically after the significant figure to which it applies (for example, 856.1 kg·m^{-3} with an uncertainty of 0.9 kg·m^{-3} is shown as 856.1 (0.9) kg·m^{-3}).

The results of the boiling point measurements on the five FAMEs are presented in Table 4. The repeatability of the pressure measurements was 0.1%. The purities of these samples were examined by a gas chromatographic method before the measurements were made.[8,14,15] In each case, the purity met or exceeded the stated purity from the supplier: methyl palmitate, 99.6%; methyl stearate, 99.7%; methyl oleate, 99.3%; methyl linoleate, 99.3%; methyl linolenate, 99.0%. Krop et al.[16] present values for the boiling point for several FAMEs, but these cannot be compared directly with our measurements since our measurements were taken at an atmospheric pressure of 83 kPa.

Table 2. Density, in kg·m^{-3}, of Two B100 Biodiesel Fuel Samples Measured at 83 kPa[a]

temperature/K	commercial sample A	commercial sample B
278.15	893.23(0.1)	892.37(0.13)
288.15	885.39(0.4)	885.00(0.10)
298.15	878.56(0.06)	877.67(0.01)
308.15	871.27(0.08)	870.36(0.05)
318.15	863.97(0.08)	863.09(0.03)
328.15	856.68(0.06)	855.62(0.41)
333.15	849.41(0.04)	848.58(0.01)

[a] The uncertainty of each measurement, discussed in the text, is the number in parentheses.

Table 3. Speed of Sound, in m·s^{-1}, of the Two Biodiesel Fuel Samples Measured at 83 kPa[a]

temperature/K	commercial sample A	commercial sample B
278.15	1468.42(0.05)	1466.85(0.56)
288.15	1431.53(0.04)	1429.87(0.61)
298.15	1395.34(0.03)	1393.60(0.68)
308.15	1359.84(0.04)	1358.05(0.75)
318.15	1324.99(0.06)	1323.17(0.90)
328.15	1290.75(0.06)	1288.86(0.90)
333.15	1257.19(0.11)	1255.36(0.96)

[a] The uncertainty of each measurement, discussed in the text, is the number in parentheses.

Table 4. Boiling Point, in K, of the Constituent FAMEs Measured at 83 kPa[a]

fluid	temperature/K	pressure/kPa
methyl palmitate	592.9(0.3)	82.82
methyl stearate	619.9(0.3)	82.76
methyl oleate	617.7(0.3)	83.62
methyl linoleate	619.0(0.3)	83.42
methyl linolenate	620.0(0.3)	82.87

[a] The uncertainty of each measurement is the number in parentheses.

Pure Fluids: Modeling

The modeling approach we used is based on equations of state (EOS). Typically, the use of an equation of state requires the critical point (critical temperature, T_c, pressure, p_c, and density, ρ_c). Experimental values of the critical parameters of the FAMEs are not available, therefore we used estimation methods. The critical temperature and pressure were estimated by use of a novel procedure based on quantitative structure−property relationship (QSPR) methodology. The procedure is described in more detail in ref[17] and is only briefly described here.

As a first step, a large-scale database of evaluated critical properties of individual compounds has been generated. Raw

(9) Bruno, T. J. *Ind. Eng. Chem. Res.* **2006**, *45*, 4371–4380.
(10) Bruno, T. J.; Smith, B. L. *Ind. Eng. Chem. Res.* **2006**, *45*, 4381–4388.
(11) Smith, B. L.; Bruno, T. J. *Ind. Eng. Chem. Res.* **2007**, *46*, 297–309.
(12) Smith, B. L.; Bruno, T. J. *Ind. Eng. Chem. Res.* **2007**, *46*, 310–320.
(13) Bruno, T. J. *Sep. Sci. Technol.* **2006**, *41*, 309–314.
(14) Bruno, T. J.; Svoronos, P. D. N., *CRC Handbook of Basic Tables for Chemical Analysis*, 2nd ed.; Taylor and Francis CRC Press: Boca Raton, FL, 2004.
(15) Bruno, T. J.; Svoronos, P. D. N., *CRC Handbook of Fundamental Spectroscopic Correlation Charts*; Taylor and Francis CRC Press: Boca Raton, FL, 2005.
(16) Krop, H. B.; Van Velzen, M. J. M.; Parsons, J. R.; Govers, H. A. J. *J. Am. Oil Chem. Soc.* **1997**, *74*, 309–315.
(17) Kazakov, A.; Muzny, C. D.; Chirico, R. D.; Diky, V. V.; Frenkel, M. Quantitative Structure-Property Relationship (QSPR) Study of Critical Properties for Pure Compounds Based on a Large Dataset Derived from Experimental Data. In *18th European Conference on Thermophysical Properties*, Pau, France, 2008.

experimental data for critical properties and their uncertainties were drawn from the NIST TRC SOURCE database.[18] For each compound with available critical temperature data, evaluated T_c was derived from all available T_c data points by use of robust regression with a Lorentzian weighting function[19] (to eliminate the influence of outliers). The evaluated critical pressure, p_c, for a given compound was obtained by use of evaluated T_c and all available experimental vapor pressure data (inclusive of boiling and triple points) by performing a 2−5 Wagner equation[20] fit, with p_c being one of the fitting parameters. Vapor-pressure data were fitted by use of robust regression techniques (MM-estimate approach of Yohai[21]). All evaluations were conducted in a batch fashion via a series of computer programs that directly interact with the database. The end result of this step was a generated database of evaluated critical temperatures for over 900 structurally diverse compounds; among them, over 700 compounds also have evaluated p_c values.

The next step was the generation of three-dimensional (3D) representations for compounds with available critical properties (i.e., compounds from the database produced during the first step) as well as for the target biodiesel components. The 3D molecular structures were obtained via optimization at the semiempirical PM3 level of theory.[22] Notable special cases are the compounds that contain long molecular chains (those also included the biodiesel components under consideration). In many practical QSPR studies, long chains in 3D molecular structures are represented with the straight conformations even though it is well-known that lower-energy conformers in such cases are "folded" under the influence of van der Waals interactions. Chain folding has a significant effect on some important molecular properties (for example, moments of inertia), and use of more physically meaningful low-energy conformers is clearly warranted. Although a comprehensive search for the lowest energy conformer was not attempted in the present study (and generally deemed ambiguous), we nevertheless conducted searches for what we term a "representative low-energy conformer." For each compound containing long chains (eight or more carbon atoms), 1000 simulated annealing calculations based on the MM3 forcefield were performed by use of the Tinker molecular mechanics package.[23] At the end of each annealing run, the final structure was further optimized by use of a PM3 Hamiltonian, and the final PM3 energy was obtained. The structure with the lowest PM3 energy obtained during the entire sequence of annealing runs was defined as the representative low-energy conformer and retained for further use.

The QSPR molecular descriptor calculations from 3D structures and subsequent correlations were carried out by use of the CODESSA package.[24] Although more general nonlinear correlations applicable to a majority of available data were sought elsewhere,[17] here we adopted a simpler but targeted approach. Specifically, for each compound that needs estimates of T_c and p_c, we draw from the database of evaluated critical properties a set of 200 compounds that are most structurally similar to this compound. A popular metric of structural similarity used in chemoinformatics is the Tanimoto index,[25] which was also used in the present study for similarity rankings. We also note that the size of the data set (200) used here to develop correlations is substantially larger that those considered in similar prior studies.[26,27]

Table 5. Estimated Critical Parameters T_c, p_c, and ρ_c of the Five FAME Compounds[a]

	methyl palmitate	methyl stearate	methyl oleate	methyl linoleate	methyl linolenate
T_c/K	755 (5)	775 (10)	782 (10)	799 (15)	772 (10)
p_c/kPa	1350 (50)	1239 (50)	1246 (50)	1341 (50)	1369 (50)
ρ_c/mol·m^{-3}	897 (7.8)	794.3 (6.7)	812.85 (7.1)	808.4 (8.5)	847.3 (9.2)

[a] The estimated uncertainty of each value is the number in parentheses.

As expected, the resulting data sets for each FAME were dominated by C/H/O molecular systems of various configurations (that constitute a majority of about 40% of the utilized experimental database). Linear correlations used to estimate properties for a specific compound were developed from the data sets of 200 similar compounds by use of the built-in CODESSA tools (e.g., the CODESSA "heuristic" method). In each case, linear correlations were generated for T_c and T_c/p_c (the ratio of T_c and p_c yields better correlations than p_c itself). High-quality correlations have been obtained in all cases, with R^2 of at least 0.97 and higher in the majority of cases. Up to eight descriptors were used in all T_c correlations, consistent with prior studies,[27] whereas three to five descriptors were found to be sufficient for T_c/p_c correlations.

After determining T_c and p_c, we used the TDE computer program[18] to estimate the value of the critical density that incorporated the density at the normal boiling point. The resulting estimates of the critical properties for the main biodiesel compounds are compiled in Table 5. The estimated uncertainties are also presented in Table 5; for comparison, the uncertainty estimates for T_c, p_c, and V_c for the recommended predictive methods, such as those incorporated into the DIPPR database for these fluids, are 5, 10, and 25%, respectively.

The equation of state is formulated in terms of the molar Helmholtz free energy as a function of density and temperature,

$$a(\rho, T) = a^0(\rho, T) + a^r(\rho, T) \quad (1)$$

where a is the molar Helmholtz energy, $a^0(\rho,T)$ is the ideal-gas contribution to the molar Helmholtz energy, and $a^r(\rho,T)$ is the real fluid molar Helmholtz energy that results from intermolecular forces. All thermodynamic properties can be calculated as derivatives of the Helmholtz energy.[28] In practical applications, the functional form used is the dimensionless Helmholtz energy, α, as a function of a dimensionless density and reciprocal temperature. The form of this equation is

$$\frac{a(\rho, T)}{RT} = \alpha(\delta, \tau) = \alpha^0(\delta, \tau) + \alpha^r(\delta, \tau) \quad (2)$$

where $\delta = \rho/\rho_c$ and $\tau = T_c/T$. The Helmholtz energy of the ideal gas is given by

(18) Frenkel, M.; Chirico, R. D.; Diky, V.; Muzny, C.; Lemmon, E. W.; Yan, X.; Dong, Q. *NIST Standard Reference Database 103, NIST ThermoData Engine: Version 3.0, Standard Reference Data*; National Institute of Standards and Technology: Gaithersburg, MD, 2008.
(19) Press, W. H.; Teukolsky, S. A.; Vetterling, S. A.; Flannery, B. P. *Numerical Recipes: The Art of Scientific Computing*, Third ed.; Cambridge University Press: New York, 2007.
(20) Wagner, W. *Cryogenics* **1973**, *13*, 470–82.
(21) Yohai, V. J. *Ann. Stat.* **1987**, *15*, 642–656.
(22) Stewart, J. J. P. *J. Comput. Chem.* **1989**, *10*, 209–220.
(23) Ponder, J. W. TINKER: Software Tools for Molecular Design, version 4.2.; URL: http://dasher.wustl.edu/tinker. 2004.
(24) CODESSA: Comprehensive Descriptors for Structural and Statistical Analysis, Version 2.0 User Manual. Semichem and University of Florida, 1995−1997.
(25) Tanimoto, T. T. *An Elementary Mathematical Theory of Classification and Prediction*; IBM Internal Report, November 17, 1958.
(26) Katritzky, A. R.; Mu, L.; Karelson, M. *J. Chem. Inf. Comput. Sci.* **1998**, *38*, 293–299.
(27) Sola, D.; Ferri, A.; Banchero, M.; Manna, L.; Sicardi, S. *Fluid Phase Equilib.* **2008**, *263*, 33–42.
(28) Span, R.; Wagner, W. *Int. J. Thermophys.* **2003**, *24*, 1–39.

$$a^0 = h_0^0 + \int_{T_0}^{T} c_p^0 \, dT - RT - T\left[s_0^0 + \int_{T_0}^{T} \frac{c_p^0}{T} \, dT - R \ln\left(\frac{\rho T}{\rho_0 T_0}\right)\right] \quad (3)$$

where ρ_0 is the ideal-gas density at T_0 and p_0 ($\rho_0 = p_0/T_0R$). The values of T_0, p_0, h_0^0, and s_0^0 are arbitrary and can be chosen based on a user's desired reference values of enthalpy and entropy. The ideal-gas Helmholtz energy is given in a dimensionless form by

$$\alpha^0 = \frac{h_0^0 \tau}{RT_c} - \frac{s_0^0}{R} - 1 + \ln\frac{\delta\tau_0}{\delta_0\tau} - \frac{\tau}{R}\int_{\tau_0}^{\tau} \frac{c_p^0}{\tau^2} \, d\tau + \frac{1}{R}\int_{\tau_0}^{\tau} \frac{c_p^0}{\tau} \, d\tau \quad (4)$$

where $\delta_0 = \rho_0/\rho_c$ and $\tau_0 = T_c/T_0$.

Equation 4 requires an expression for the ideal-gas heat capacity c_p^0 of each of the pure fluids. Experimental information was not available; therefore, we used the predictive methods in the TDE computer program[18] to estimate values of the ideal-gas heat capacity. Values for the ideal-gas heat capacity were estimated by use of the method of Joback and Reid[29] with group parameters re-evaluated at NIST/TRC[30] and then fitted to the following "Planck−Einstein" form used in reference equations of state:[31,32]

$$c_p^0 = c_0 T^{c_1} + c_2\frac{(c_3/T)^2 \exp(c_3/T)}{[1 - \exp(c_3/T)]^2} + c_4\frac{(c_5/T)^2 \exp(c_5/T)}{[1 - \exp(c_5/T)]^2} + c_6\frac{(c_7/T)^2 \exp(c_7/T)}{[1 - \exp(c_7/T)]^2} \quad (5)$$

In eq 5, the temperature is in units of K, and c_p^0 is in units of $J \cdot mol^{-1} \cdot K^{-1}$. This form can extrapolate reliably to high temperatures that may be of interest in fuels applications and is superior to common polynomial fits that often have unphysical behavior when extrapolated beyond the range over which they were fitted. The resulting values of the coefficients for eq 5 are given in Table 6; the estimated uncertainty of c_p^0 calculated with eq 5 and these coefficients is 10%, due mainly to the uncertainty associated with the method of Joback and Reid.[29]

One of the most common functional forms used for the residual Helmholtz energy equation of state for a pure fluid is

$$\alpha^r(\delta,\tau) = \sum n_k \delta^{i_k}\tau^{j_k} + \sum n_k \delta^{i_k}\tau^{j_k}\exp(-\delta^{l_k}) \quad (6)$$

where the summation is over the polynomial and exponential terms in the equation, and where each summation typically contains 4−20 terms. The form used in this work has 13 terms plus additional Gaussian bell-shaped terms similar to the Lemmon et al. equation of state for propane,[33]

$$\alpha^r(\delta,\tau) = \sum_{k=1}^{5} N_k \delta^{d_k}\tau^{t_k} + \sum_{k=6}^{10} N_k \delta^{d_k}\tau^{t_k}\exp(-\delta^{l_k}) + \sum_{k=11}^{13} N_k \delta^{d_k}\tau^{t_k}\exp(-\eta_k(\delta - \varepsilon_k)^2 - \beta_k(\tau - \gamma_k)^2) \quad (7)$$

This form can represent not only the vapor pressure and density, but also other properties, such as the speed of sound (which can have a noticeable impact on injection timing for the pump-line-nozzle fuel-injection systems used on some diesel engines).[34] All of these thermodynamic properties can be expressed in terms of the Helmholtz energy. The development of the functional form of the equation is described by Lemmon.[35]

Another feature of this particular formulation is that although uncertainty in the critical values propagates directly into the uncertainty of the critical region of the equation of state, it will not greatly affect properties outside of the critical region that are based on regressing experimental data. This is in contrast to some of the simple equations of state that have parameters expressed in terms of the critical parameters; these can be much more sensitive to the values of the critical parameters used.

Typically, the Helmholtz-energy form requires a large amount of high-quality experimental data in order to determine the multiple parameters of the equation. A feature of the new form of the Helmholtz energy equation and the regression procedure[35] is that a significant number of thermodynamic constraints are imposed that allow even very limited experimental data to be used to develop a well-behaved equation that extrapolates in a physically reasonable manner. Since the coefficients of the equation are empirical, in cases with very limited data it is possible to obtain a set of coefficients that results in unphysical behavior (such as negative heat capacities at low temperatures) in regions where data are unavailable. The use of appropriate constraints in the regression removes this problem.

In an earlier work[8] we performed an extensive literature survey to locate experimental data that included data compilations such as the DIPPR database[36] and the TDE database.[18] The experimental data are summarized in Table 7; the uncertainties for the properties are those ascribed by the TDE program. Details on the procedure for obtaining these uncertainty estimates are in ref 30.

Pure Fluids: Results

The experimental data given in Table 7 were used in a multiproperty regression procedure to obtain the coefficients and

(29) Joback, K. G.; Reid, R. C. *Chem. Eng. Commun.* **1987**, *57*, 233–243.
(30) Frenkel, M.; Chirico, R. D.; Diky, V.; Yan, X. J.; Dong, Q.; Muzny, C. *J. Chem. Inf. Model.* **2005**, *45*, 816–838.
(31) Wagner, W.; Pruβ, A. *J. Phys. Chem. Ref. Data* **2002**, *31*, 387–535.
(32) Lemmon, E. W.; Jacobsen, R. T. *J. Phys. Chem. Ref. Data* **2005**, *34*, 69–108.
(33) Lemmon, E. W.; McLinden, M. O.; Wagner, W. , *J. Chem. Eng. Data* **2009**, in press.
(34) Tat, M. E.; Van Gerpen, J. H. *Measurement of Biodiesel Speed of Sound and Its Impact on Injection Timing, Report NREL/SR-510−31462*; National Renewable Energy Laboratory: Golden, CO, 2003.
(35) Lemmon, E. W. Fitting 14-Term Equations of State with Just Two Data Points, paper 597. In *17th International Symposium on Thermophysical Properties*: Boulder CO, 2009.
(36) Rowley, J. R., Wilding, W. V., Oscarson, J. L., Rowley, R. L. *DIADEM, DIPPR Information and Data Evaluation Manager*, version 3.0, sponsor release Aug. 2008; Brigham Young University: Provo, UT, 2004.
(37) Haller, A.; Youssofian, A. *C.R. Acad. Sci.* **1906**, *143*, 803–806.
(38) Scott, T. A.; Macmillan, D.; Melvin, E. H. *Ind. Eng. Chem.* **1952**, *44*, 172–175.
(39) Verkade, P. E.; Coops, J. *Biochem Z.* **1929**, *206*, 468–481.
(40) Spizzichino, C. *J. Rech. C. N. R. S.* **1956**, *34*, 1–24.
(41) Sauer, J. C.; Hain, B. E.; Boutwell, P. W. *Org. Synth.* **1940**, *20*, 67.
(42) Swern, D.; Knight, H. B.; Jordan, E. F. *Biochem. Prep.* **1960**, *7*, 84.
(43) Niemann, C.; Wagner, C. D. *J. Org. Chem.* **1942**, *7*, 227.
(44) Meer, W. A.; Jannke, P. J. *J. Pharm. Soc.* **1961**, *50*, 204–207.
(45) Whitmore, F. C.; Sutherland, L. H.; Cosby, J. N. *J. Am. Chem. Soc.* **1942**, *64*, 1360–1364.
(46) Rose, A.; Supina, W. R. *J. Chem. Eng. Data* **1961**, *6*, 173.
(47) Norris, F. A.; Terry, D. E. *Oil Soap* **1945**, *22*, 41–46.

Table 6. Value of the Coefficients c_0−c_7 in Eq 5 for the Five FAMEs

	methyl palmitate	methyl stearate	methyl oleate	methyl linoleate	methyl linolenate
c_0	120.529	247.115	90.2385	190.986	79.5913
c_1	0.080 1627	−0.091 6606	0.146 118	0.020 213	0.214 648
c_2	345.62	276.94	234.797	437.371	290.379
c_3	2952.37	556.17	613.529	3052.11	1213.24
c_4	289.038	408.997	335.768	287.222	81.4323
c_5	734.653	1311.85	1405.31	746.631	578.752
c_6	301.639	472.702	431.66	321.956	474.881
c_7	1593.55	2825.71	2867.76	1624.33	2799.79

exponents given in Tables 8 and 9. The regression procedure includes thermodynamic consistency constraints in addition to constraints on the shapes and limiting behavior of various curves obtained from taking derivatives of the Helmholtz energy (details are in given by Lemmon[35]). Average absolute deviations (AAD = 100 × abs[θ_{exp}−θ_{calc}]/θ_{exp}), where θ is the property of interest, are given in Table 7 for each property for each fluid. The quantity of experimental data for all of the FAMEs investigated was limited; methyl palmitate, methyl stearate, and methyl oleate had the most data, whereas methyl linoleate and methyl linolenate had extremely sparse data sets. In addition, there often were large deviations between different sources that exceeded the estimated uncertainty of the data; this was especially true for vapor-pressure data. Figure 1 demonstrates this problem for the vapor pressure of methyl palmitate. For temperatures above 400 K, the equation of state represents the data to within the uncertainty bands of most of the experimental data; however, the uncertainties are rather large. Below 400 K, there are two data sets[40,57] that disagree significantly. Additional experimental data can help resolve these differences; however, at such low temperatures it is very difficult to obtain vapor-pressure data with low uncertainties. To help remedy this situation, our regression procedure uses other types of data when available, such as heats of vaporization and heat capacity, along with thermodynamic consistency, to guide the behavior of the vapor-pressure curve at low temperatures.

Mixture Model. For calculations of the thermodynamic properties of mixtures, we use a mixture model explicit in Helmholtz energy that can utilize any equation of state, provided that it can be expressed in terms of the Helmholtz energy.[86] This form of model has been used successfully for refrigerant mixtures[86] and for natural gas mixtures.[87] Details on the mixture model are given in refs 86 and 88. The pure fluid equations of state and the mixture model were implemented into the REFPROP[89] computer program. We are unaware of any other equation-of-state-based approaches that focused on thermodynamic properties of biodiesel such as density and sound speed, although there have been recent equation-of-state-based approaches to modeling the solubility of water in biodiesel.[90]

The basic idea is to represent the molar Helmholtz energy, a, of a mixture as a sum of an ideal contribution, a^{id}, and an excess contribution, a^{excess}, according to:

$$a = a^{id} + a^{excess} \tag{8}$$

$$a^{id} = \sum_{j=1}^{m} x_i[a_i^0(\rho, T) + a_i^r(\delta, \tau) + RT \ln x_i] \tag{9}$$

$$a^{excess} = RT \sum_{i=1}^{m-1} \sum_{j=i+1}^{m} x_i x_j F_{ij} \sum_k N_k \delta^{d_k} \tau^{t_k} \exp(-\delta^{l_k}) \tag{10}$$

where ρ and T are the mixture molar density and temperature; δ and τ are the reduced mixture density and temperature; m is

(48) Vederame, F. D.; Miller, J. G., III *J. Phys. Chem.* **1962**, *66*, 2185–2188.
(49) Althouse, P. M.; Hunter, G. W.; Triebold, H. O. *J. Am. Oil Chem. Soc.* **1947**, *24*, 257–259.
(50) Klykov, V. N.; Serebrennikova, G. A.; Perobrazhenskii, N. A. *Z. Org. Khim.* **1966**, *2*, 1782–1785.
(51) Bonhorst, C. W.; Althouse, P. M.; Triebold, H. O. *Ind. Eng. Chem.* **1948**, *40*, 2379.
(52) Goodwin, S. R.; Newsham, D. M. T. *J. Chem. Eng. Data* **1975**, *20*, 180.
(53) Dauben, W. G. *J. Am. Oil Chem. Soc.* **1948**, *70*, 1376.
(54) Cason, J.; Wolfhagen, H. J.; Targey, W.; Adams, R. E. *J. Org. Chem.* **1949**, *14*, 147–154.
(55) Zhang, G. S. *Synth. Commun.* **1998**, *28*, 1159–1162.
(56) Cason, J.; Allinger, N. L.; Summrell, G.; Williams, D. E. *J. Org. Chem.* **1951**, *16*, 1170–1176.
(57) Van Genderen, A. C. G.; van Miltenburg, J. C.; Van Bommel, M. J.; van Ekeren, P. J.; van den Berg, G. J. K.; Oonk, H. A. J. *Fluid Phase Equlibria* **2002**, *202*, 109–120.
(58) Nevin, C. S.; Althouse, P. M.; Triebold, H. O. *J. Am. Oil Chem. Soc.* **1951**, *28*, 325–327.
(59) Eykman, J. F. *Natuurkd. Verh. Hollandsche Maatschappij Wet. Haarlem* **1919**, *8*, 438–555.
(60) Gouw, T. H.; Vlugter, J. C. *J. Am. Oil Chem. Soc.* **1964**, *41*, 142–145.
(61) Drake, N. L.; Spies, J. R.; Cotton Resin, I. I. I. *J. Am. Chem. Soc.* **1935**, *57*, 184–187.
(62) Rusling, J. F.; Bertsch, R. J.; Barford, R. A.; Rothbart, H. L. *J. Chem. Eng. Data* **1969**, *14*, 169–173.
(63) Gaikwad, B. R.; Subrahmanyam, V. V. R. *J. Ind. Chem. Soc.* **1988**, *65*, 266–268.
(64) Gros, A. T.; Feuge, R. O. *J. Am. Oil Chem. Soc.* **1952**, *29*, 313.
(65) Lipkind, D.; Kapustin, Y.; Umnahanant, P.; Chickos, J. S. *Thermochim. Acta* **2007**, *456*, 94–101.
(66) van Miltenburg, J. C.; Oonk, H. A. J.; Van Bommel, M. J. *J. Chem. Eng. Data* **2004**, *49*, 1036–1042.
(67) Gouw, T. H.; Vlugter, J. C. *J. Am. Oil Chem. Soc.* **1964**, *41*, 524–526.
(68) Murray, K. E.; Schoenfeld, R. *J. Am. Oil Chem. Soc.* **1952**, *29*, 416–420.
(69) Menzel, W.; Berger, A.; Nikuradse, A. *Verhalten von Fettsaureestern in Electrischen Entladungen Chemische Berichte- Recueil* **1949**, *82*, 418–425.
(70) Boelhouwer, J. W. M.; Nederbragt, G.; Verberg, G. W. *Appl. Sci. Res. Sect. A.* **1950**, *2*, 249.
(71) Rose, A.; Schrodt, V. N. *J. Chem. Eng. Data* **1964**, *9*, 12–16.
(72) Greaves, W. S.; Linstead, R. P.; Shepard, B. R.; Thomas, S. L. S.; Weedon, B. C. L. *J. Chem. Soc. (London)* **1950**, *332*, 6–3330.
(73) Mumford, S. A.; Phillips, J. W. C. *J. Chem. Soc. (London)* **1950**, 75–84.
(74) Shreve, O. D.; Heether, M. R.; Knight, M. R.; Swern, H. B. *Anal. Chem.* **1950**, *22*, 1498.
(75) Mitrofanova, T. K.; Gusev, V. D.; Preobrazhenskii, N. A.; Investigations in the field of lipids, X. L. *J. Org. Chem. U.S.S.R.* **1966**, *2*, 1748–1750.
(76) Hosman, B. B. A.; Van Steenis, J.; Waterman, H. I. *Recl. Trav. Chim. Pays-Bas* **1949**, *68*, 939.
(77) Liew, K. Y.; Seng, C. E. *J. Am. Oil Chem. Soc.* **1992**, *69*, 734–740.
(78) Cueto, M. J. M.; Vallejo, M. G.; Luque, V. F. *Grasas Aceites (Seville)* **1991**, *42*, 14–21.
(79) Simmons, H. E.; Smith, R. D. *J. Am. Chem. Soc.* **1959**, *81*, 4256.
(80) Bridgman, P. W. *Proc. Am. Acad. Arts Sci.* **1932**, *67*, 1–27.
(81) Knegtel, J. T.; Boelhouwer, C.; Tels, M.; Waterman, H. I. *J. Am. Oil Chem. Soc.* **1957**, *34*, 336–337.
(82) Keffler, L.; McLean, J. H. *J. Soc. Chem. Ind.* **1935**, *54*, 178–185.
(83) Albert, O. *Z. Phys. Chem. (Munich)* **1938**, *182*, 421.
(84) Wheeler, D. H.; Riemenschneider, R. W. *Oil Soap* **1939**, *16*, 207–209.
(85) Fuchs, R.; Peacock, L. A. *Can. J. Chem.* **1980**, *58*, 2796.

Table 7. Summary of Experimental Data for FAMEs

reference	npts	*T*/K	*p*/kPa	unc.%	AAD, %	reference	npts	*T*/K	*p*/kPa	unc. %	AAD, %
a. Summary of Experimental Data for Methyl Palmitate											
Vapor Pressure											
Haller and Youssofian[37]	1	469	2	40	12.2	Scott et al.[38]	7	378−445	0.01−0.8	1−4	4.0
Verkade and Coops[39]	1	450	1.2	45	16.6	Spizzichino[40]	17	309−375	1×10^{-5}−0.01	20	66.9
Sauer et al.[41]	3	390−455	0.1−1.3	25−30	25.8	Swern et al.[42]	1	435	0.5	53	7.7
Niemann and Wagner[43]	1	436	0.7	20	17.3	Meer and Jannke[44]	1	439	0.7	81	10.5
Whitmore et al.[45]	1	436	0.7	81	18.8	Rose and Supina[46]	12	467−516	1.9−9.3	8−30	4.1
Norris and Terry[47]	5	409−470	0.1−2.7	2−23	8.2	Verderame and Miller[48]	1	467	1.6	35	27.8
Althouse et al.[49]	1	425	0.3	52	15.2	Klykov et al.[50]	1	401	0.1	126	8.5
Bonhorst et al.[51]	7	422−475	0.3−2.7	2−19	3.5	Goodwin and Newsham[52]	6	464−497	1.9−6.4	8−22	4.5
Dauben[53]	1	406	0.04	30	162.4	Krop et al.[16]	3	447−595	0.7−99.6	14−60	21.1
Cason et al.[54]	1	439	0.5	24	13.8	Zhang[55]	1	450	0.7	85	49.5
Cason et al.[56]	1	436	0.5	56	6.5	van Genderen et al.[57]	31	303−361	1e-5−0.005	5−100	10.8
Nevin et al.[58]	2	421−458	0.3−1.3	20−48	7.1	this work	1	593	83	0.1	0.04
Density											
Eykman[59]	1	354	sat	0.2	0.24	Gouw and Vlugter[60]	1	313	sat	0.1	0.23
Drake and Spies[61]	1	293	sat	0.1	1.44	Rusling et al.[62]	1	298	sat	0.6	1.99
Bonhorst et al.[51]	3	311−372	101	0.6	0.05	Gaikwad and Subrahmanyam[63]	5	333−353	101	0.6	0.06
Gros and Feuge[64]	1	348	sat	0.1	0.28	Ott et al.[8]	7	308−338	83	0.1	0.04
Heat of Vaporization											
Lipkind et al.[65]	1	298	sat	1	1.8						
Heat Capacity											
van Miltenburg et al.[66]	5	310−350	101	0.3	1.9						
Sound Speed											
Gouw and Vlugter[67]	1	313	101	0.14	0.26	Ott et al.[8]	7	308−338	83	0.1	0.04
b. Summary of Experimental Data for Methyl Stearate											
Vapor Pressure											
Haller and Youssofian[37]	1	488	2	41	9.3	Nevin et al.[58]	2	441−481	0.27−1.33	20−48	9.2
Verkade and Coops[39]	1	476	1.5	45	22.7	Murray and Schoenfeld[68]	1	425	0.13	25	29.6
Niemann and Wagner[43]	1	439	0.2	25	2.2	Scott et al.[38]	12	399−467	0.02−0.80	1−4	1.8
Norris and Terry[47]	5	428−495	0.1−2.7	2−23	8.7	Spizzichino[40]	18	327−393	2×10^{-5}−0.01	31−44	21.0
Althouse et al.[49]	1	447	0.27	52	11.5	Swern et al.[42]	1	454	0.53	55	20.2
Bonhorst et al.[51]	6	443−480	0.27−1.33	4−20	6.6	Meer and Jahnke[44]	1	456	0.67	81	30.6
Menzel[69]	1	436	0.07	30	157.2	Rose and Supina[46]	11	477−513	1.27−4.8	6−14	4.2
Boelhouwer et al.[70]	1	452	0.4	60	5.1	Rose and Schrodt[71]	12	427−485	0.11−1.74	6−92	5.5
Greaves et al.[72]	2	383−409	0.01−0.04	30	31.8	Klykov et al.[50]	1	421	0.08	113	9.4
Mumford and Phillips[73]	1	473	1.3	20	25.0	Krop et al.[16]	2	493−620	2−99.6	10−80	14.4
Shreve et al.[74]	1	453	0.5	25	23.9	Zhang[55]	1	474	0.93	68	10.0
Cason et al.[56]	1	454	0.5	56	14.0	van Gederen et al.[57]	14	316−359	1×10^{-5}−0.001	10−100	7.0
Mitrofanova[75]	1	474	1.2	13	14.7	this work	1	620	83	0.1	0.01
Density											
Bonhorst et al.[51]	3	310−372	sat	0.6	0.08	Gouw and Vlugter[60]	1	313	sat	0.1	0.07
Hosman et al.[76]	1	313	sat	0.6	0.05	Gaikwad and Subrahmanyam[63]	5	333−353	sat	0.6	0.11
Boelhouwer et al.[70]	5	323−513	sat	0.1	0.19	Ott et al.[8]	5	318−338	83	0.1	0.02
Gros and Feuge[64]	1	348	sat	0.1	0.01	Liew and Seng[77]	9	313−353	101	0.7-.8	0.02
Cueto et al.[78]	1	313	sat	0.1	2.04						
Heat of vaporization											
Lipkind et al.[65]	1	298	sat	1	1.62						
Heat Capacity											
van Miltenburg et al.[66]	4	320−350	101	0.3	2.24						
Sound Speed											
Ott et al.[8]	5	318−338	83	0.1	0.07	Gouw and Vlugter[67]	1	313	101	0.13	0.29
c. Summary of Experimental Data for Methyl Oleate											
Vapor Pressure											
Haller and Youssofian[37]	1	486	2	40	0.35	Rose and Schrodt[71]	38	429−487	0.13−1.9	2−5	8.95
Whitmore et al.[45]	1	448	0.7	80	72.9	Klykov et al.[50]	1	405	0.03	260	6.15
Norris and Terry[47]	5	426−491	0.1−2.7	2−22	6.3	Krop et al.[16]	1	619	101	25	17.6
Shreve et al.[74]	1	453	0.5	25	7.6	Lipkind et al.[65]	4	300−450	8×10^{-7}−0.37	20−25	27.29
Scott et al.[38]	10	401−458	0.03−0.63	2−4	0.93	this work	1	618	0.083	0.1	0.01
Simmons and Smith[79]	1	403	0.05	166	62.1	Mitrofanova et al.[75]	1	411	0.02	80	62.26
Density											
Bridgman[80]	25	273−368	98−980665[a]		0.91	Ott et al.[8]	7	278−338	83	0.1	0.02
Knegtel et al.[81]	1	293	101	0.15	0.11	Keffler and McLean[82]	4	288−303	101	0.1	0.01
Gouw and Vlugter[60]	2	293−313	101	0.1	0.04	Mitrofanova et al.[75]	1	297	101	0.1	1.9
Albert[83]	4	293−453	101	0.6	0.24	Wheeler and Riemenschneider[84]	2	293−298	101	0.6	0.01
Heat of vaporization											
Fuchs and Peacock[85]	1	298	sat	2	0.15	Lipkind et al.[65]	1	298	sat	1.5	0.43
Sound Speed											
Gouw and Vlugter[67]	2	293−313	101	0.1	0.11	Ott et al.[8]	7	278−338	83	0.1	0.02
d. Summary of Experimental Data for Methyl Linoleate											
Vapor Pressure											
Norris and Terry[47]	5	423−488	0.1−2.7	2	18.9	Krop et al.[16]	1	619	101	25	17.6
Scott et al.[38]	10	392−458	0.01−0.65	1.5	0.85	Lipkind et al.[65]	4	300−450	5×10^{-7}−0.2	20−30	87.4
Klykov et al.[50]	1	409	0.03	243	39.8	this work	1	619	83	0.1	0.0
Density											
Gouw and Vlugter[60]	2	293−313	101	0.1	0.14	Ott et al.[8]	7	278−338	83	0.1	0.02
Heat of vaporization											
Lipkind et al.[65]	1	298	sat	1	0.09						
Sound Speed											
Ott et al.[8]	7	278−338	83	0.1	0.04	Gouw and Vlugter[67]	2	293−313	101	0.13	0.25
e. Summary of Experimental Data for Methyl Linolenate											
Vapor Pressure											
Scott et al.[38]	9	394−459	0.016−0.627	1.5−5	44.09	Lipkind et al.[65]	4	300−450	3×10^{-7}−0.2	20−30	65.6
Klykov et al.[50]	1	406	0.041	190	53.73	this work	1	620	83	0.1	0.0

Table 7. Continued

reference	npts	*T*/K	*p*/kPa	unc.%	AAD, %	reference	npts	*T*/K	*p*/kPa	unc. %	AAD, %
Krop et al.[16]	1	620	101	25	18.12						
Density											
Gouw and Vlugter[60]	2	293−313	101	0.1	0.13	Ott et al.[8]	7	278−338	83	0.1	0.03
Heat of Vaporization											
Lipkind et al.[65]	1	298	sat	1	0.64						
Sound Speed											
Ott et al.[8]	7	278−338	83	0.1	0.05	Gouw and Vlugter[67]	1	293−313	101	0.1	0.10

[a] Measurements were obtained as relative volumes; data above atmospheric pressure not used in development of correlation.

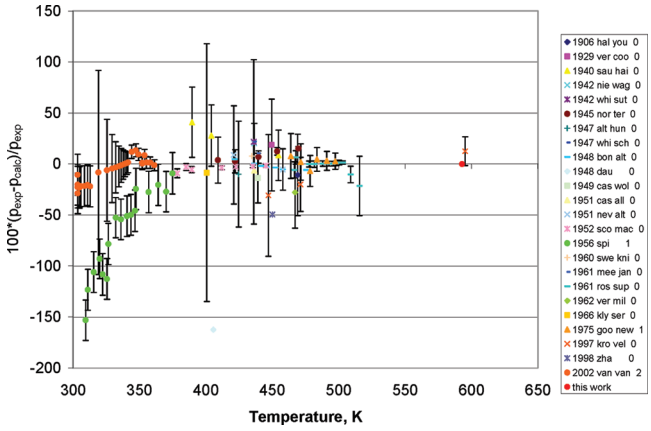

Figure 1. Comparison of the vapor pressure calculated from the equation of state and experimental data for methyl palmitate.

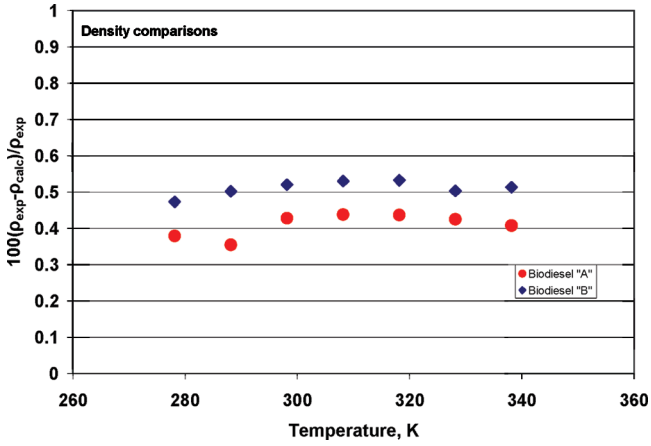

Figure 2. Comparison of the density calculated from the equation of state mixture model and experimental data for B100 biodiesel fuel samples.

Table 8. Coefficients for Gaussian Bell-shaped Terms in the Equation of State, Eq 7

k	η_k	β_k	γ_k	ϵ_k
11	1.1	0.90	1.14	0.79
12	1.6	0.65	0.65	0.90
13	1.1	0.75	0.77	0.76

the number of components; a_i^0 is the ideal-gas Helmholtz energy of component *i*; a_i^r is the residual (or real-fluid) Helmholtz energy of component *i*; the x_i are the mole fractions of the constituents

(86) Lemmon, E. W.; Jacobsen, R. T. *J. Phys. Chem. Ref. Data* **2004**, *33*, 593–620.

(87) Kunz, O.; Klimeck, R.; Wagner, W.; Jaeschke, M. *The GERG-2004 Wide-Range Reference Equation of State for Natural Gases and Other Mixtures*; GERG Technical Monograph; Fortschr.-Ber. VDI, VDI-Verlag: Düsseldorf Germany, 2007.

(88) Lemmon, E. W.; McLinden, M. O. Method for Estimating Mixture Equation of State Parameters, In *Thermophysical Properties and Transfer Processes of New Refrigerants Conference*, Paderborn Germany, 2001; International Institute of Refrigeration, Commission B1: Paderborn, Germany, 2001; pp 23−30.

Table 9. Coefficients and Exponents of the Equation of State, Eq 7, for FAMEs

k	N_k	t_k	d_k	l_k
	a. Methyl Palmitate			
1	$0.428\,282\,1 \times 10^{-01}$	1	4	0
2	$0.244\,316\,2 \times 10^{+01}$	0.36	1	0
3	$-0.375\,754\,0 \times 10^{+01}$	1.22	1	0
4	−0.158 852 6	1.45	2	0
5	$0.405\,599\,0 \times 10^{-01}$	0.7	3	0
6	$-0.152\,409\,0 \times 10^{+01}$	3	1	2
7	−0.768 616 7	3.9	3	2
8	$0.179\,995\,0 \times 10^{+01}$	2.2	2	1
9	$-0.159\,096\,7 \times 10^{+01}$	2.9	2	2
10	$-0.126\,768\,1 \times 10^{-01}$	1.25	7	1
11	$0.219\,834\,7 \times 10^{+01}$	2.6	1	2
12	−0.773 721 1	3.0	1	2
13	−0.431 452 0	3.2	3	2
	b. Methyl Stearate			
1	$0.395\,963\,5 \times 10^{-01}$	1	4	0
2	$0.246\,665\,4 \times 10^{+01}$	0.3	1	0
3	$-0.389\,595\,0 \times 10^{+01}$	1.25	1	0
4	−0.116 737 5	1.65	2	0
5	$0.412\,722\,9 \times 10^{-01}$	0.8	3	0
6	$-0.140\,373\,4 \times 10^{+01}$	3.1	1	2
7	−0.646 526 4	3.4	3	2
8	$0.193\,467\,5 \times 10^{+01}$	2.3	2	1
9	$-0.160\,812\,4 \times 10^{+01}$	3.8	2	2
10	$-0.111\,381\,3 \times 10^{-01}$	1.2	7	1
11	$0.212\,532\,5 \times 10^{+01}$	3.2	1	2
12	−0.777 267 1	3.8	1	2
13	−0.418 368 4	3.8	3	2
	c. Methyl Oleate			
1	$0.459\,612\,1 \times 10^{-01}$	1	4	0
2	$0.229\,540\,0 \times 10^{+01}$	0.34	1	0
3	$-0.355\,436\,6 \times 10^{+01}$	1.14	1	0
4	−0.229 167 4	1.4	2	0
5	$0.685\,453\,4 \times 10^{-01}$	0.6	3	0
6	$-0.153\,577\,8 \times 10^{+01}$	3.3	1	2
7	−0.733 469 7	4.1	3	2
8	$0.171\,270\,0 \times 10^{+01}$	1.9	2	1
9	$-0.147\,139\,4 \times 10^{+01}$	3.8	2	2
10	$-0.172\,467\,8 \times 10^{-01}$	1.3	7	1
11	$0.211\,547\,0 \times 10^{+01}$	3.4	1	2
12	−0.755 537 4	3.8	1	2
13	−0.413 426 9	4	3	2
	d. Methyl Linoleate			
1	$0.318\,318\,7 \times 10^{-01}$	1	4	0
2	$0.192\,728\,6 \times 10^{+01}$	0.2	1	0
3	$-0.368\,505\,3 \times 10^{+01}$	1.2	1	0
4	0	1	2	2
5	$0.8449312 \times 10^{-01}$	1	3	3
6	−0.9766643	2.2	1	1
7	−0.4323178	2.5	3	3
8	$0.2000470 \times 10^{+01}$	1.8	2	2
9	$-0.1752030 \times 10^{+01}$	1.92	2	2
10	$-0.1726895 \times 10^{-01}$	1.47	7	7
11	$0.2116515 \times 10^{+01}$	1.7	1	1
12	−0.7884271	2.3	1	2
13	−0.3811699	2.1	3	2
	e. Methyl Linolenate			
1	$0.407\,082\,9 \times 10^{-01}$	1	4	0
2	$0.241\,237\,5 \times 10^{+01}$	0.15	1	0
3	$-0.375\,619\,4 \times 10^{+01}$	1.24	1	0
4	−0.152 646 6	1.6	2	0
5	$0.468\,291\,8 \times 10^{-01}$	1.28	3	0
6	$-0.147\,095\,8 \times 10^{+01}$	2.9	1	2
7	−0.764 550 0	3.15	3	2
8	$0.190\,896\,4 \times 10^{+01}$	2.16	2	1
9	$-0.162\,936\,6 \times 10^{+01}$	2.8	2	2
10	$-0.124\,207\,3 \times 10^{-01}$	1.4	7	1
11	$0.218\,070\,7 \times 10^{+01}$	2.5	1	2
12	−0.753 726 4	3	1	2
13	−0.434 778 1	3.1	3	2

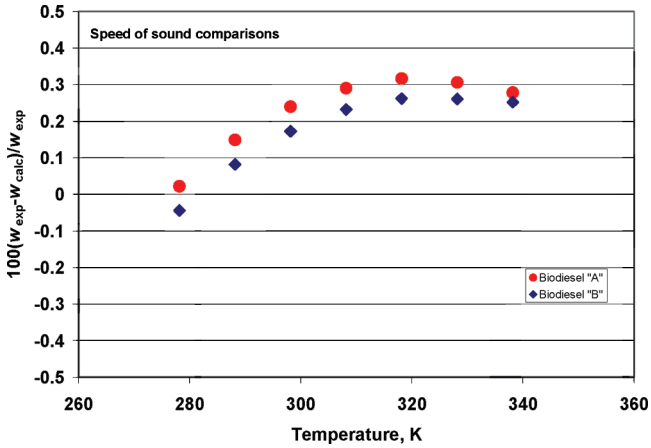

Figure 3. Comparison of the speed of sound calculated from the equation of state mixture model and experimental data for B100 biodiesel fuel samples.

of the mixture; d_k, t_k, l_k, and N_k are coefficients found from fitting experimental data; and F_{ij} is an interaction parameter. Mixing rules are used to determine the reducing parameters ρ_{red} and T_{red} for the mixture, which are defined as

$$\delta = \rho/\rho_{red} \tag{11}$$

$$\tau = T_{red}/T \tag{12}$$

$$\rho_{red} = \left[\sum_{i=1}^{m} \frac{x_i}{\rho_{c_i}} + \sum_{i=1}^{m-1}\sum_{j=i+1}^{m} x_i x_j \xi_{ij}\right]^{-1} \tag{13}$$

$$T_{red} = \sum_{i=1}^{m} x_i T_{c_i} + \sum_{i=1}^{m-1}\sum_{j=i+1}^{m} x_i x_j \varsigma_{ij} \tag{14}$$

where ξ_{ij} and ς_{ij} are binary interaction parameters that define the shapes of the reducing temperature and density curves.

The model has a total of three binary interaction parameters—ξ_{ij}, ς_{ij}, and F_{ij}—that can be determined by fitting experimental data, when available. For the binary mixtures in this work, binary mixture data were unavailable. However, the FAMEs studied here are similar in chemical structure, and as a first approximation we set all binary interaction parameters to a default value of zero. Future work on binary mixtures of FAMEs can explore the validity of this assumption.

Mixture Model Results. After normalizing the compositions for the two B100 biodiesel fuel samples given in Table 1, we calculated the density and speed of sound at a pressure of 83 kPa (the local atmospheric pressure in Boulder, Colorado, USA). Figures 2 and 3 compare the model and experimental B100 data for density and speed of sound, respectively. The calculated density is within 0.6% of the experimental values, and the calculated sound speed is within 0.4% of the experimental values. Although this exceeds the experimental uncertainty of 0.1%, we feel these results demonstrate that the modeling approach is very promising. Future work on binary mixtures may improve the representation of the density and sound speed by permitting the use of binary interaction parameters determined from regressing experimental data. However, as all of the constituent FAMEs used in the model are similar in size and chemical nature, we do not expect large contributions from binary interactions.

In addition, we calculated the bubble point temperature at 83 kPa. The bubble point temperature[91] is the temperature of the saturated liquid phase at a given pressure, when the very first "bubble" of vapor is about to form. The model calculated a bubble point of 614.4 K (at 83.2 kPa) for biodiesel sample "A" and 614.2 K (at 83.5 kPa) for sample "B". This compares well with experimental values[7] of 616.6 K (at 83.2 kPa) for sample A and 615.6 K (at 83.5 kPa) for sample B. However, when we calculated the entire distillation curve, we observed that our calculations were systematically low compared to the experimental values,[7] and the deviations became greater as the distillation progressed. We cannot presently explain the inability of our model to represent the full distillation curve; work to resolve this issue is in progress. It is possible that the distillation curve is particularly sensitive to heavy components that occur in small amounts that we have not included in our analysis. It is also possible that some dimerization occurs at the higher temperatures encountered in the later stages of the distillation curve.[92] Such a chemical change cannot at present be accounted for in the model.

Conclusions

We developed preliminary equations of state based on limited experimental data for methyl palmitate, methyl stearate, methyl oleate, methyl linoleate, and methyl linolenate. The equations behave in a physically reasonable manner at extrapolated conditions and can be used for temperatures to 700 K and pressures to 50 MPa. These equations were used in a mixture model to calculate the density, sound speed, and bubble point of two samples of commercial B100 biodiesel fuels and compared well with our experimental measurements. The density is represented to within 0.6% and the sound speed to within 0.4%, demonstrating the applicability of the model. The bubble point is predicted to within 0.4%. The model presented here allows one to predict the themodynamic properties of any biodiesel fuel whose composition can be expressed in terms of the five FAMEs: methyl palmitate, methyl stearate, methyl oleate, methyl linoleate, and methyl linolenate. Future work is planned to explore the properties of additional biodiesel samples, the modeling of the full distillation curve, and binary mixtures of the constituent FAMEs. In particular, we must address the issue of compositional variability, which is an important factor in all fuels research. This can be done as additional orthogonal fuel samples become available for study.

Acknowledgment. We gratefully acknowledge the financial support of the NASA/Glenn Research Center under agreement NNC98 VB55P.

EF900159G

(89) Lemmon, E. W.; Huber, M. L.; McLinden, M. O. *NIST Standard Reference Database 23, NIST Reference Fluid Thermodynamic and Transport Properties Database (REFPROP)*, version 8.0, Standard Reference Data; National Institute of Standards and Technology: Gaithersburg, MD, 2007.

(90) Oliveira, M. B.; Varanda, F. R.; Marrucho, I. M.; Queimada, A. J.; Coutinho, J. A. P. *Ind. Eng. Chem. Res.* **2008**, in press.

(91) Himmelblau, D. M., *Basic Principles and Calculations in Chemical Engineering*, Third ed.; Prentice-Hall, Inc.: Englewood Cliffs, NJ, 1974.

(92) Waynick, J. A. *Characterization of Biodiesel Oxidation and Oxidation Products, Task 1 Results, Technical Literature Review, SwRI Project no. 08−10721*; National Renewable Energy Laboratory, NREL/TP-540−39096: Golden, CO, 2005.